Acta Acustica united with Acustica
Vol. 103 (2017) 987 – 997

DOI 10.3813/AAA.919128

Visualization of Delaminations in Composite Structures Using a Baseline-Free, Sparse Array Imaging Technique Based on Nonlinear Lamb Wave Propagation

Morteza Tabatabaeipour, Jan Hettler, Steven Delrue, Koen Van Den Abeele
Wave Propagation and Signal Processing, Department of Physics, KU Leuven Campus
Kulak 8500 Kortrijk, Belgium. koen.vandenabeele@kuleuven.be

Summary
Environmental factors such as temperature and humidity influence the efficacy of defect imaging procedures based on the identification of changes between an intact state and the current state of a sample/component/structure in the presence of a defect. In this paper, we focus on the Reconstruction Algorithm for Probabilistic Inspection of Damage (RAPID) and propose a nonlinear Lamb wave version of RAPID to visualize a delamination in a composite structure without having to know anything about the intact state, i.e. a baseline free RAPID. Once the optimal frequency selection of Lamb waves in a pitch-catch configuration mode is performed, low and high excitation amplitude signal responses within a sparse array at that frequency are evaluated along each transducer-receiver path by analyzing a set of damage sensitive parameters: the correlation coefficient, the energy of the scaling subtracted signal, and the third harmonic ratio. Processing of this information leads to a corresponding probabilistic damage map of the area within the sparse array. The obtained results from a validation experiment demonstrate the capability of this nonlinear variant of RAPID for the identification of a delamination in a composite structure.

PACS no. 43.25.-x, 43.35.Zc, 43.60.-c

1. Introduction

Nonlinear Non-Destructive Testing (NDT) is a fairly new research area in the field of ultrasonic NDT. Consequently, imaging techniques based on the nonlinear response of defects in materials have not been fully developed yet. Nonetheless, some interesting and thought-provoking results have been reported recently, and typically, a distinction is made between local nonlinear imaging techniques, which require some sort of surface scanning, and nonlocal ones. As an example of a local nonlinear imaging technique, internal (subsurface) defects have been detected by mapping the distribution of nonlinearity in the signals measured point-by point on the sample surface, e.g. using a Scanning Laser Doppler Vibrometer (S-LDV) in response to an external excitation [1, 2]. Time reversal (TR) imaging is a second example of a local nonlinear imaging technique, where nonlinear scatterers can be identified by focusing high levels of energy on the sample surface using TR and by subsequently measuring the modulation of a high-frequency ultrasonic wave by a low-frequency vibration on the cracked surface using LDV [3].

Received 5 April 2017,
accepted 27 September 2017.

Concerning the nonlocal imaging techniques, Kazakov *et al.* [4] demonstrated that cracks are truly nonlinear scattering sources as the amplitude and phase of the signals reflected from a crack are modulated, whereas linear scatterers such as a hole or inclusion show no modulation. Analysis of the reflections in combination with a continuous low frequency excitation allows us to create images in which nonlinear scattering sources can be distinguished from other scatterers. More recently, Ohara *et al.* [5] developed a novel imaging technique called the Subharmonic Phased Array for Crack Evaluation (SPACE) based on subharmonic waves and phased array processing to measure closed stress corrosion cracks in the reactor mantle of a nuclear power plant. All of the above methods are based on a modification of an existing (linear) ultrasonic measuring technique by explicitly considering the contribution of nonlinearity in the response signals.

In this paper, we focus on another interesting defect imaging technique called Reconstruction Algorithm for Probabilistic Damage Inspection (RAPID) [6, 7] and we intend to modify it such that it accounts for nonlinearity in the wave propagation. In conventional RAPID, defects are imaged by comparing the data collected by a permanent array of ultrasonic transducers, between an intact and a damaged state. This method is capable of visualizing defects,

provided the defect lies within the sensor network. One of the main limitations however is the availability of the response of the intact system ("baseline") under the same conditions as the "current" or "damaged" state recordings. In the present research study, a baseline-free RAPID imaging method based on an analysis of the nonlinear ultrasonic wave propagation characteristics is introduced, and its feasibility is evaluated using experimental data for a delamination defect. In preparation of this, we recall the most important aspects of nonlinear mesoscopic elastic material behavior in Section 2 and introduce the experimental setup in Section 3. Section 4 presents a novel dispersion curve based empirical technique for optimal frequency selection, in order to carry out nonlinear Lamb wave measurements in pitch-catch experiments. The knowledge of the optimal frequency range is crucial in the performance of the nonlinear Lamb wave imaging method using the baseline-free RAPID concept.

2. Nonlinear mesoscopic elastic material

It has been demonstrated by several researchers that atomic elastic materials, once they are damaged, respond similar to nonlinear mesoscopic elastic (NME) materials, such as rock and concrete. In contrast to intact materials which may inherently possess a form of atomic nonlinear elasticity, NME materials exhibit nonlinear mesoscopic elasticity [8, 9, 10, 11, 12]. Whereas atomic or classical nonlinear elasticity can be described by a higher order expansion of stress versus strain attributed to an asymmetry in the intermolecular potential, nonclassical nonlinearity of NME materials arises from hysteresis in the stress–strain response due to the presence of a multitude of internal contacts or damage [13], which gives rise to ultrasonic wave distortion. This classical and nonclassical nonlinear wave distortion can be evidenced by a resonance frequency shift with increasing excitation amplitude [14, 15], nonlinear attenuation [16], wave modulation [17], and generation of higher harmonics [14, 18].

Hysteresis effects may result from clapping or internal friction in "low-aspect ratio" features such as cracks, grain boundaries, and delaminations. The particular dynamic behavior of these features absorbs energy, resulting in attenuation of the sound wave, and in the creation of nonclassical nonlinear waves [4]. For example, the appearance of hysteresis in the stress-strain relation can be the result of a transition between static (stick mode) and kinetic (slide mode) friction under the action of a harmonic shear deformation [19]. During dynamic straining, the period of the contact stiffness varies twice within the period of the input strain, generating odd higher harmonics [20, 21]. Validation experiments and simulations have indeed demonstrated that even harmonics cannot be generated in a pure hysteretic system [16, 22, 23].

The various experimental and theoretical methods, initially developed for the validation and description of nonclassical nonlinear wave propagation in metals, rocks and concrete, can also be employed in the study of composite materials containing a delamination. In the following, we will first determine an optimal excitation frequency providing a highly sensitive Lamb wave-delamination interaction by analyzing the response of a short pulse signal. Next, we demonstrate that the dissipation of energy and the generation of harmonics in response to a single 'optimal' frequency excitation can be interpreted as a source of nonlinearity. This level of nonlinearity will then be further quantified in order to reconstruct an image of the nonlinear source, such as a closed delamination in this research study, using an updated version of the classical RAPID imaging algorithm that properly accounts for the presence and the degree of the nonlinearity.

3. Specimen and experimental setup

The sparse array RAPID experiment will be carried out on a composite sample with dimensions 300 × 300 × 2.76 mm^3. A delamination type defect has been introduced during manufacturing using an insert of Teflon with dimensions 20 × 20 mm^2 located at ¾th of the sample thickness. The $[(0, 45)_3]_S$ laminate consists of 12 laminas with an identical thickness of 0.23 mm and a density of 1490 kg/m^3. The basic linear elasticity tensor C of each lamina provided by the manufacturer is represented in Equation (1) in GPa units, assuming transverse isotropy,

$$\begin{bmatrix} 58.7 & 5.5 & 4.1 & 0 & 0 & 0 \\ 5.5 & 58.7 & 4.1 & 0 & 0 & 0 \\ 4.1 & 4.1 & 11.1 & 0 & 0 & 0 \\ 0 & 0 & 0 & 2.4 & 0 & 0 \\ 0 & 0 & 0 & 0 & 2.4 & 0 \\ 0 & 0 & 0 & 0 & 0 & 3.9 \end{bmatrix}. \quad (1)$$

The elastic tensor and all other material constants are used to obtain the theoretical dispersion curves using the GUIGUW software [24] in order to compare with the empirical dispersion curves.

The plate is equipped with a sparse array network consisting of nine DuraAct patch P-876/SP1 transducers with a diameter of 10 mm and a thickness of 0.4 mm, see Figure 1. Signal excitation is performed using a NI-PXI-5421, 16-Bit arbitrary waveform generator card. The received signals are digitized by NI-PXI-5122 high speed digitizers with a sampling rate of 10 MS/s. For the signal amplification on excitation, a 1 channel power amplifier (Falco systems) with a frequency range up to 5 MHz, and a maximum output of ±100 V_{pp} was used. The measurement system is fully controlled by NI-LabVIEW software.

4. Lamb waves: Pitch-catch optimal defect frequency (PC-ODF) selection technique

In view of an optimal realization of the RAPID technique based on nonlinear Lamb wave propagation, and considering the fact that a sparse array measurement system (as used in RAPID) is only capable of measuring signals in

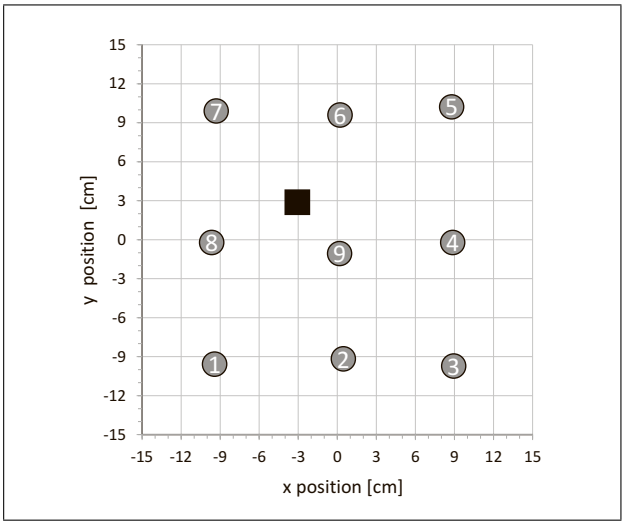

Figure 1. Arrangement of the transducers within the sparse array network on the composite plate used for nonlinear Lamb wave imaging. The numbered circles indicate the position of the transducers, as well as their ordering in the sparse array measurement. The position of the delamination is represented by the black square.

a pitch-catch configuration, we first need to search for a frequency at which a strong interaction between the Lamb wave and the defect occurs. Typically, this interaction is manifested by a pronounced attenuation in the pitch-catch measurement. Once the Pitch-Catch Optimal Defect Frequency (PC-ODF) range is identified, it will further be used for the new nonlinear baseline-free imaging concept.

To illustrate the procedure of finding the PC-ODF range for Lamb waves in a pitch-catch configuration, an exploratory experiment, prior to the RAPID experiment, is conducted using a LDV line-scanning acquisition as a response to an excitation by a DuraAct patch P-876/SP1 along two lines on the composite surface. The schematic configuration for the measurement of the optimal frequency selection technique is shown in Figure 2.

A broadband excitation (0.5 cycle, 750 kHz) is successively fed into each of the transducers. Using a motorized LDV, the received out-of-plane signals are measured along both the intact and the delaminated path, and the acquired signals are processed using 2D-FFT in order to obtain frequency–wavelength (f–k) images, corresponding to the calculation [25]

$$H(k, f) = \left| \iint u(x,t) \mathrm{e}^{-\mathrm{j}(\omega t + kx)} \, \mathrm{d}x \, \mathrm{d}t \right|, \qquad (2)$$

where $u(x,t)$ is the particle displacement of the points on the plate and $H(k,f)$ is the 2D-FFT (in modulus) of $u(x,t)$. ω and k are angular frequency and wavenumber respectively.

The results of this transformation are shown in Figure 3. Note that the dominant dispersion curves for the Lamb modes (symmetric Lamb modes are indicated by the letter S, anti-symmetrical by the letter A) are in agreement with Giurgiutiu and Pohl's findings regarding the amplitude of the fundamental Lamb wave modes generated by a

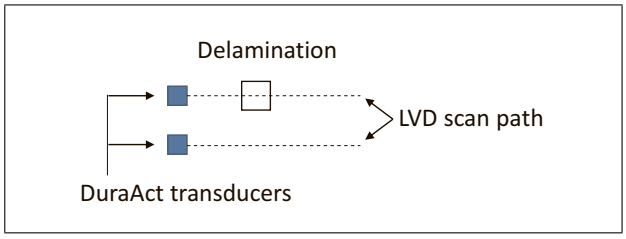

Figure 2. Schematic configuration using an LDV line scan measurement for optimal Lamb wave frequency selection. Two scan paths are considered: one crossing the delamination, the other over an intact zone.

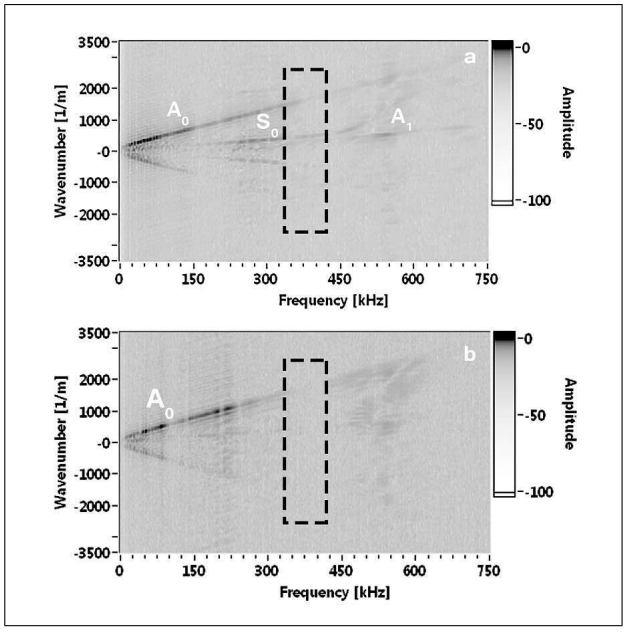

Figure 3. Frequency-Wavenumber ($f-k$) images shown in dB units obtained after analysis of signals acquired in response to a 0.5 cycle, 750 kHz excitation, considering a) a path through the intact region, and b) a path through the damaged region. The results show the dissipation of the high frequency content in the second case (delamination region), particularly in the range of 350–410 kHz.

bonded piezo-actuator [26, 27, 28]: The A_0 mode is dominant in the early part of the dispersion curve, whereas the S0 mode dominates at higher frequencies. Clearly, the high frequency content is strongly attenuated when the broadband excitation propagates through the delamination zone.

The broadband 2D-FFT analysis can be utilized for the evaluation of the excitability, the attenuation, and the sensitivity to defects (basic factors introduced by Wilcox *et al.* [29]), and thus for the selection of the optimal excitation frequency. Therefore, it can also be exploited for the proper Lamb wave mode tuning in practical NDT applications when a piezo is attached on a structure. Using the 2D-FFT data (Equation 2), one can easily determine the dispersion curves of the dominant modes at each frequency for further analysis of the wavenumber and the phase velocity dispersion by applying Equations (3) and (4),

$$K(f) = \max_k H(k, f), \qquad (3)$$

$$C_p(f) = 2\pi f / K(f). \quad (4)$$

Figure 4 illustrates the dominant wavenumber versus frequency results. It is apparent that S_0 and the higher order Lamb modes such as A_1, which dominate the high frequency response (> 250 kHz) on the intact path, are generally overruled by the A_0 wave mode response on the delaminated zone. Moreover, whereas the S_0 mode dominates within the frequency range of 350–410 kHz along the intact path, this mode has almost completely vanished when evaluating the propagation through the delamination zone. Mensil *et al.* introduced this instantaneous wavenumber (IW) technique for the first time and showed that the dominating wavenumber is increasing when analyzing signals measured above a delamination zone in comparison with the intact zone behavior [30]. The results visualized in Figures 4a and 4b confirm this phenomenon. For instance, for an excitation frequency in the range of 250–340 kHz, which is a range of intermediate sensitivity, the S_0 wave mode is repressed by a higher wavenumber wave mode (A_0) when traveling through the delamination zone, which is in accordance with Figure 6a in the paper of Mensil *et al.* [30]. Above 410 kHz, similar repression by the higher wavenumber A_0 mode is found for S_0 and for A_1.

To complete the information, a narrowband frequency excitation analysis has also been conducted. Figure 5 displays for instance the amplitude reduction when exciting the sample using a long sine burst at 378 kHz. We observe that the out-of-plane displacement of the S_0 mode (observed on the intact path) totally disappears when considering the same excitation signal passing through the delamination zone. A severe amplitude dissipation of 97.6% is observed at this frequency.

In conclusion, we can safely state that the band 350–410 kHz is a highly sensitive frequency range as any mode excitation completely disappears. The adjacent bands of 250–350 kHz and 410–700 kHz are bands with intermediate sensitivity (modes exist, but the dominance changes) while the range of frequencies below 250 kHz can be regarded as an insensitive range (no change in mode dominance).

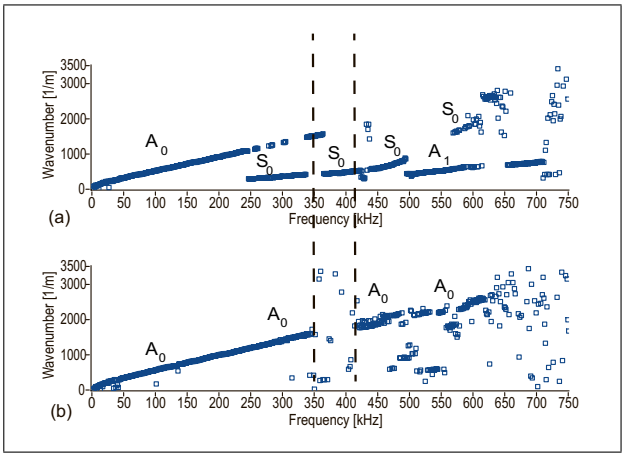

Figure 4. Wavenumber dispersion curves of the dominant wave modes obtained after analysis of signals acquired in response of a 0.5 cycle, 750 kHz excitation using the DuraAct P-876/SP1 patch transducer, considering a) a path through the intact region, and b) a path through the damaged region. The results confirm the complete disappearance of modes in the highly sensitive range of 350–410 kHz, and a mode shift to A_0 mode in the range of 250–350 kHz and 410–700 kHz. There is no apparent sensitivity to the defect in the lower frequency band ≤ 250 kHz.

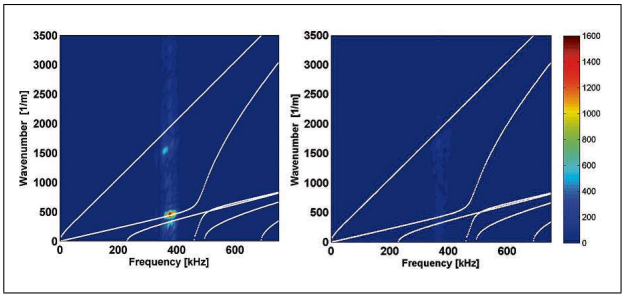

Figure 5. (Colour online) Frequency-Wavenumber ($f-k$) image comparison in response to a narrowband frequency excitation at 378 kHz. a) intact path b) path running through the delamination zone, illustrating the extreme amplitude reduction of the out-of-plane displacement for the S_0 mode. The theoretical dispersion curves based on the (linear) elastic tensor given in equation (1) are plotted in white on top of the ($f-k$) image.

5. Nonlinear signal difference coefficient (NSDC)

Nonlinearity in the wave propagation manifests itself in different ways. One way to explore the presence of nonlinearity is to evaluate the sample response after being excited at multiple levels of pulse amplitudes. If nonlinearity is present, the response to a high and low amplitude level excitation will be different. The difference between the two signals, either due to frequency shifts, phase shifts, nonlinear attenuation or harmonic generation, will then serve as an indicator of nonlinearity (linked to a damage feature) in the sample. This is quite interesting for the RAPID algorithm, since 1) the response to different amplitude levels can be obtained subsequently without having to account for environmental changes, and 2) the nonlinear response is damage selective.

Whereas the conventional RAPID concept is essentially based on the calculation of a path dependent signal difference coefficient (SDC) between the "intact" or "baseline" and the "current" or "damaged" signals, the newly proposed RAPID concept will substitute these terms by the "low amplitude excitation response" and the "high amplitude excitation response", respectively. The difference between the latter two responses will be the basis of the definition of a nonlinear signal difference coefficient (NSDC). Various formulations for the NSDC can be chosen, involving operations such as the correlation coefficient, the scaling subtraction, or the third harmonic analysis. Apart from replacing the SDC by one of the proposed NSDC's, the

RAPID procedure used in the original version remains the same [6, 7].

5.1. Nonlinear imaging using the correlation coefficient

The signal difference coefficient for nonlinear imaging based on the correlation coefficient for the path $i \to j$ (i.e. between transducer i and receiver j) can be defined as

$$\rho_{ij} = \frac{\mathrm{Cov}\left(r^l_{ij}(t), r^h_{ij}(t)\right)}{\mathrm{SD}\left(r^l_{ij}(t)\right)\mathrm{SD}\left(r^h_{ij}(t)\right)}, \quad (5)$$

$$\mathrm{NSDC}_{ij} = 1 - \rho_{ij}, \quad (6)$$

where $r^l_{ij}(t)$, $r^h_{ij}(t)$ are the received signals at low and high excitation amplitude level, respectively, whereas Cov and SD represent the covariance of the signals and their standard deviation. It should be mentioned that the correlation coefficient is not primarily sensitive to a pure amplitude variation. On the other hand, the correlation coefficient turns out to be a suitable and damage sensitive parameter when either the frequency or the time of flight are changing within the signals under comparison. Both frequency broadening due to harmonic generation and phase shifts are features that may be induced by nonlinearity, and therefore, the proposed NSDC can be considered as an excellent parameter that can be used in the new nonlinearity based imaging concept. Low values of NSDC_{ij} indicate a rather linear transducer–receiver path $i \to j$ (the difference is potentially noise dominated), whereas non-zero values refer to the presence of damage along the path.

5.2. Nonlinear imaging using the Scaling Subtraction Method (SSM)

A second indicator of nonlinearity is simply the lack of scalability of its response. If the response of a system exactly scales with the amplitude of the excitation, the system can be considered to be linear. Nonlinear systems exhibit a lack of scalability in the received signals which can be easily tested by acquiring two responses at high and low excitation levels. If nonlinearity is present, the two responses, after rescaling the low amplitude signal by the ratio of the excitation levels, will be different. The difference between the high and the rescaled low amplitude signals, which is called the SSM signal, can be used as an indicator of nonlinearity (linked to a damage feature) in the sample.

In practice, the measured signals are first rescaled in order to eliminate the amplitude variation in the acquired signals. This rescaling operation can be implemented as

$$X(t)_s = \frac{X(t) - \mathrm{offset}}{\mathrm{scale}}, \quad (7)$$

where $X(t)$ is the measured signal, and offset and scale are expressed as

$$\mathrm{offset} = X(t)_{\min} + \mathrm{scale}, \quad (8)$$

$$\mathrm{scale} = \frac{X(t)_{\max} - X(t)_{\min}}{2}. \quad (9)$$

The SSM signal is then simply obtained by a subtraction of the scaled high and low amplitude responses as expressed in Equation (10). Finally, by calculating the energy of the SSM signal, we obtain the expression for the second damage sensitive nonlinear indicator (Equation 11).

$$\mathrm{SSM}_{ij}(t) = r^h_{ij,s}(t) - r^l_{ij,s}(t), \quad (10)$$

$$\mathrm{NSDC}_{ij} = \frac{1}{nT}\int_0^{nT} \mathrm{SSM}^2_{ij}(t). \quad (11)$$

Here, $r^h_{ij,s}(t)$ and $r^l_{ij,s}(t)$ are the scaled high and low amplitude signal respectively, and nT is an integer multiple of the signal period. As in the case of the correlation coefficient, this SSM damage indicator is highly sensitive to time of flight and frequency variations.

5.3. Nonlinear imaging using the third harmonic ratio signature

The appearance of a delamination between lamina of a composite structure is usually accompanied by frictional slip at the contacting interfaces when excited by an oscillating tangential traction. As mentioned in Section 2, this phenomenon naturally results in the generation of odd harmonics, which all are proportional to the square of the fundamental amplitude [16]. Therefore, the evaluation of the level of the third harmonic in the high amplitude signals $r^h_{ij}(t)$ can also be considered as a measure of "damage induced nonlinear signal difference" (assuming that the low amplitude excitation is not activating the friction, and thus, its response is free of harmonics). As such, a third option for the formulation of the NSDC_{ij} can be expressed as

$$\mathrm{NSDC}_{ij} = \left(\frac{A_3}{A_1^2}\right)_h \quad (12)$$

where A_3 and A_1 are, respectively, the third harmonic and fundamental amplitude of the high amplitude response. The subscript h refers to the high amplitude signal $r^h_{ij}(t)$.

If a system is purely linear, noiseless and exhibits no nonlinear behavior, the NSDC_{ij} value is theoretically zero. However, if there is a source of nonlinearity inside the sample, e.g. a delamination defect, the NSDC_{ij} values may vary for specific transmitter-receiver pairs depending on the nonlinearity encountered on the propagation path. In reality, any composite sample, even an intact one, will not behave purely linear. Consequently, the NSDC_{ij} values are not necessarily zero for intact paths as well. Nevertheless, we expect to see a far larger nonlinearity in the damaged paths with respect to the intact paths. This last remark is of course valid for any of the NSDC formulations (Equations 6, 11 and 12).

6. Amplitude-dependent response of the NSDC in a composite containing a delamination

In order to construct a probabilistic image based on the nonlinearity generated by the interaction of defects with

Lamb waves in a sparse network of transducers, we recall from Section 4 that the frequency of 378 kHz was found to be the pitch-catch optimal defect frequency for the considered composite plate containing the delamination (introduced in Section 3). The acquired signals at this optimal frequency showed a strong interaction with the delamination defect, manifested by a 97.6% amplitude reduction in the out-of-plane displacement on the surface of structure measured by LDV. Therefore, 378 kHz was selected as the excitation frequency, and Hanning-windowed 250-cycle tone burst signals of 378 kHz were fed into the DuraAct transducers of the sparse array network in a round-robin fashion.

After selection of a suitable low level excitation, the amplitude levels for the high amplitude excitation (before amplification) were varied from $q = 0.4\,\mathrm{V}$ to $q = h = 2\,\mathrm{V}$. Response signals were measured at these different excitation levels for further nonlinear investigations, revealing amplitude-dependent curves for the cross correlation coefficient (14), the energy of the SSM signal (15) and the nonlinear third harmonic ratio (16) over each transducer-receiver path. According to Scalerandi *et al.*, the initial part of the response signal (near the arrival time) is the best part of the signal to be analyzed for nonlinearity using multiple signal techniques [9]. In view of this, a signal length of $n = 125$ periods is therefore used in this study when calculating the correlation coefficient and the energy of the SSM signal. For a signal at 378 kHz, the period T equals 2.64 µs.

Thus, based on the acquired signals (with $i, j = 1..9$)

$$r_{ij}^{l}(t), \quad l = 0.2\,\mathrm{V}, \tag{13}$$
$$r_{ij}^{q}(t), \quad q = 0.4, 0.6, \ldots, h = 2\,\mathrm{V},$$

we probe

$$\rho_{ij}(q) = \frac{\mathrm{Cov}\left(r_{ij}^{q}(t), r_{ij}^{l}(t)\right)}{\mathrm{SD}\left(r_{ij}^{q}(t)\right)\mathrm{SD}\left(r_{ij}^{l}(t)\right)}, \tag{14}$$

$$\mathrm{SSM}_{ij}(q) = \frac{1}{nT}\int_{0}^{nT}\left[\rho_{ij,s}^{q}(t) - \rho_{ij,s}^{l}(t)\right]^{2}, \tag{15}$$

$$\mathrm{THR}_{ij}(q) = \left(\frac{A_3}{A_1^2}\right)_q \tag{16}$$

as function of the excitation level q. Note that the excitation levels mentioned in this Section are the input values before amplification. For the real amplitude levels that were fed into the transducer, the excitation levels should be multiplied by a factor of 50.

Eventually, for the construction of the images, it suffices to select two suitable low and high excitation levels for the calculation of the NSDC values over each transducer-receiver path, as explained in the previous section.

However, before evaluating the aforementioned damage sensitive parameters for the entire set of experimental data obtained by the sparse array network, we first discuss one representative case showing paths 1 → 5 (T1R5) and 3 → 7 (T3R7) as an example of an intact and a damage path, respectively, both with a propagation distance of 28.2 cm. The measured 'high amplitude' signals (corresponding to $q = h = 2\,\mathrm{V}$) in both paths are compared in Figure 6. A strong 67% amplitude reduction due to the delamination is apparent in Figure 6a. Furthermore, Figure 6b and 6c compare the high (2 V) and properly scaled low level (0.2 V) response signals in both paths. Nonlinear attenuation and a phase shift can be readily observed in the delamination path. In a detailed study of the scaling subtraction method (SSM), Bruno *et al.* demonstrated the occurrence of three primary phenomena, consisting of 1) amplitude variation, 2) phase variation, and 3) higher harmonic generation [31]. The relatively small drop in amplitude between the high amplitude response signal and the up-scaled low level response for an intact path is potentially caused by a moderate level of higher harmonic

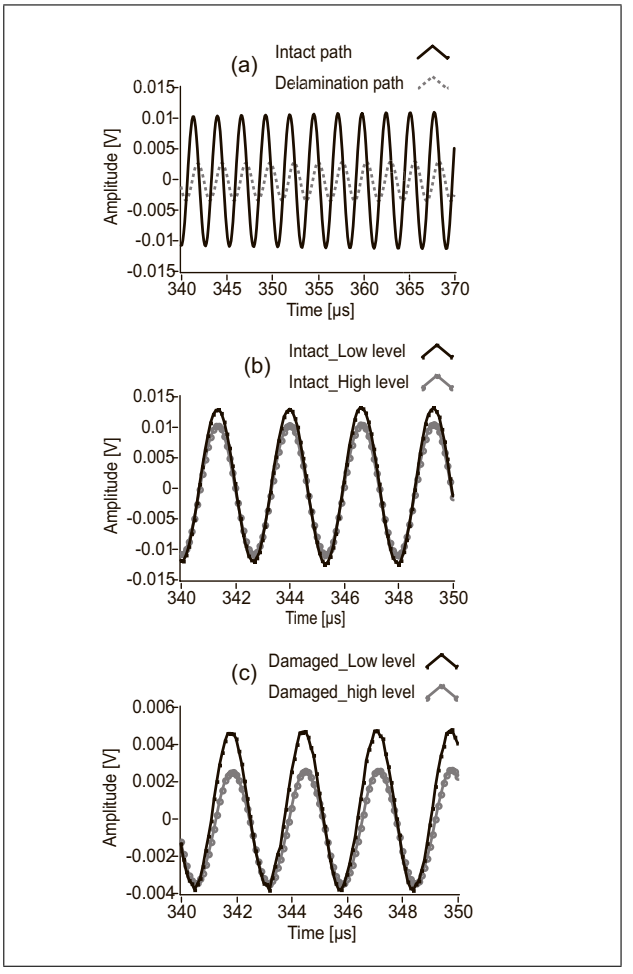

Figure 6. Comparison of the acquired signals along an intact path (T1R5) and along a damaged path (T3R7) a) comparison of the intact and damaged path response signals for an excitation level of 2 V showing a strong 67% amplitude reduction due to the delamination, b) high amplitude ($q = h = 2\,\mathrm{V}$) and properly up-scaled low level ($q = l = 0.2\,\mathrm{V}$) response signals upon traveling over the intact path, c) high amplitude ($q = h = 2\,\mathrm{V}$) and properly up-scaled low level ($q = l = 0.2\,\mathrm{V}$) response signals upon traveling over the damaged path. The comparison reveals a high level of nonlinear attenuation and a phase shift of the signal propagating through the delamination (c) compared to the intact state (b).

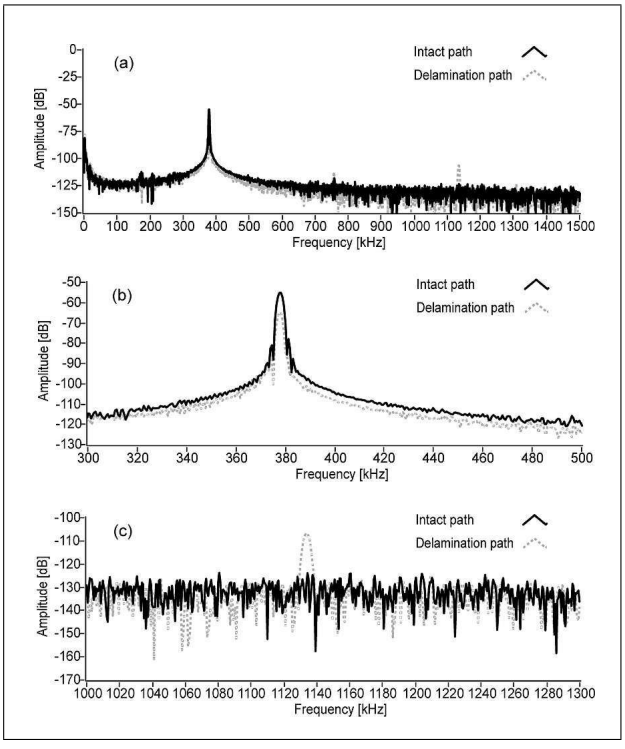

Figure 7. Spectral analysis of response signals acquired on intact (T1R5) and delaminated paths (T3R7) at a high level of excitation ($q = h = 2$ V), showing a 9.5 dB amplitude reduction in the fundamental amplitude and a 19.9 dB increase in the third harmonic amplitude. a) Complete amplitude spectrum, b) close-up image near the fundamental frequency, c) close-up image near the third harmonic component.

generation due to the classical nonlinearity of the material and instrumentation (see Figure 6b). However, the amplitude drop observed in Figure 6c is far larger and should therefore be attributed to the nonlinear attenuation and the shift of energy towards the generation of higher harmonics induced by frictional effects at the location of the delamination. We will discuss these phenomena in more detail in the following figures.

The spectral analysis of the response signals acquired over the intact path and over the delamination path at a high level of excitation (2 V), shows that there is a 9.5 dB amplitude reduction in the fundamental component (see Figure 7). On the other hand, there is a 19.9 dB increase in the third harmonic component due to the presence of the delamination. As mentioned in Section 2, the increase of odd harmonics can be attributed to hysteretic effects induced by friction, occurring at the delamination zone. Figure 7a additionally reveals that hysteresis has little effect on the even harmonics, which are primarily related to the anharmonicity of the elastic energy [23].

The difference between linear and nonlinear attenuation for signals traveling on the intact and damaged paths can be observed in Figure 8. Van Den Abeele *et al.* have demonstrated that an analysis of the kinetic energy loss may be a simple way to verify whether hysteresis is present in a material or not. In their study, they have also emphasized that the loss due to hysteresis should not be

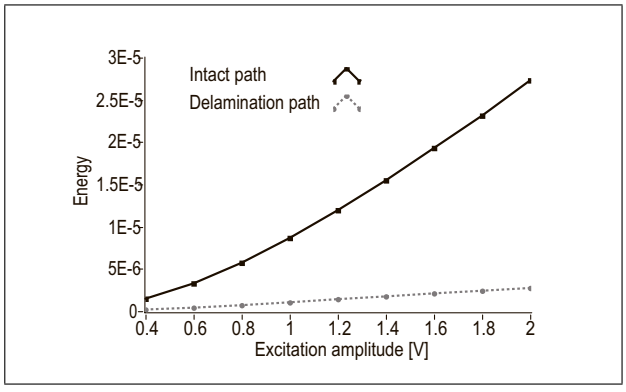

Figure 8. Excitation amplitude dependence of the energy of measured signals that traveled on the intact (T1R5) and damaged paths (T3R7) analyzed from experimental data obtained at 378 kHz, showing linear and nonlinear attenuation in the delamination path (T3R7).

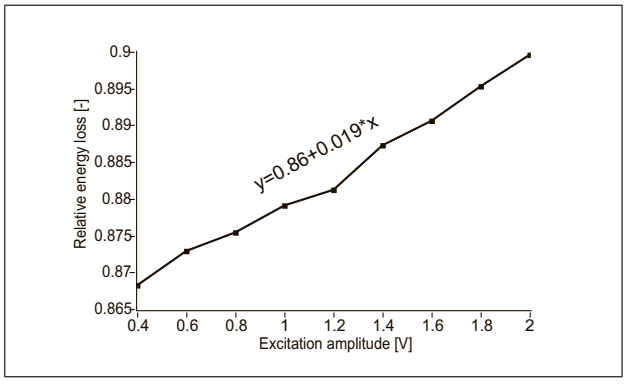

Figure 9. Relative energy loss as function of the excitation amplitude (measured at 378 kHz), illustrating a vast increase of energy loss, proportional to the excitation amplitude.

confused with the apparent 'classical' nonlinear loss in the fundamental due to harmonic generation [16]. To verify the energy loss, they defined the following relative energy loss (REL) metric:

$$\mathrm{REL} = \left| \frac{E_d - E_i}{E_i} \right|, \tag{17}$$

where E_d and E_i are the energy of the signals traveling along the damaged and intact paths, respectively. Figure 8 illustrates, on one hand, that the absolute energy of the damaged signal at all excitation levels is much lower than the energy of the intact signal, and, on the other hand, that the proportionality rate E_d/E_i is substantially reduced as the excitation amplitude increases. In Figure 9, the relative energy loss is displayed, showing a vast increase of the energy loss, proportional with the excitation amplitude, when considering the path that goes through the delamination in comparison with the intact path. This supports the idea of hysteresis behavior across the delamination path in the presence of linear attenuation.

The nonlinear phenomena occurring in the delamination path can be further displayed by examining the various nonlinear damage indicators we have introduced in

the previous section. Figure 10 illustrates the behavior of the correlation coefficient parameter as function of the excitation amplitude, which can be calculated from Equation (14). Clearly the coherence between the low (reference) signal response and the high amplitude signal response is decreasing with increasing excitation amplitude for response signals acquired after traveling through the delamination path, whereas this correlation coefficient is approximately constant, around a value equal to 1, for the analysis over the intact path.

The second damage indicator we have introduced was the SSM signal energy (Equation 15). Figure 11 shows the excitation amplitude dependence of the energy of the SSM signals, after rescaling, applying Equations (7)–(9) and thus only retaining the effects of phase shift and/or frequency variation when comparing the lowest level signal to the different high amplitude signals. The SSM energy values for the delamination path are clearly increasing with increasing excitation amplitude, whereas the results for the intact path are constant. This fully supports the results obtained in the analysis of the correlation coefficient.

Albeit for a completely different application, the above results are also found to be in line with a study reported by Rivière *et al.* on osseointegration monitoring [32]. In this study, the authors compared the sensitivity of three parameter dependencies, namely the correlation coefficient, the time delay and the energy of the SSM signal as function of input excitation levels, to probe the nonlinearity at an interface between a prosthesis and the bone. Similar amplitude dependencies as shown in Figure 10 and 11 were obtained. Further, in order to simulate linear and nonlinear cases, they considered load-carrying implants to bone connections with different tightness levels, and concluded that the nonlinearity of the system is decreasing as the tightness level is increasing. Their analysis results show that the correlation coefficient (coherence) is increasing as the nonlinearity of the system is decreasing. Similarly, the phase shift (derived from the time delay) is decreasing along with a decrease in the nonlinearity of the system. In addition, the energy of the SSM signal gradually decreases as the system becomes more and more linear. If one identifies in the current study the intact path T1R5 as a linear system and the delamination path T3R7 as a nonlinear system, the results displayed in Figure 10 and 11 illustrate a similar behavior for the damage sensitive parameters related to the correlation coefficient and the energy of the SSM signal.

Finally, as a third option for a damage sensitive indicator, we have analyzed the amplitude dependence of the third harmonic spectral components for the intact and delamination paths. Assuming hysteresis (e.g. due to friction) is the dominant mechanism for nonlinearity, the third harmonic component should be proportional to the square of the fundamental [16]. Therefore, in accordance with Equation (16), the ratio of the third harmonic component to the square of the fundamental was calculated for both intact and damaged states. This ratio should be constant, and the larger the value of the ratio, the larger the nonlinearity for the system. Figure 12 indeed confirms the expectation of a higher third harmonic ratio for the delaminated path in comparison with the intact path.

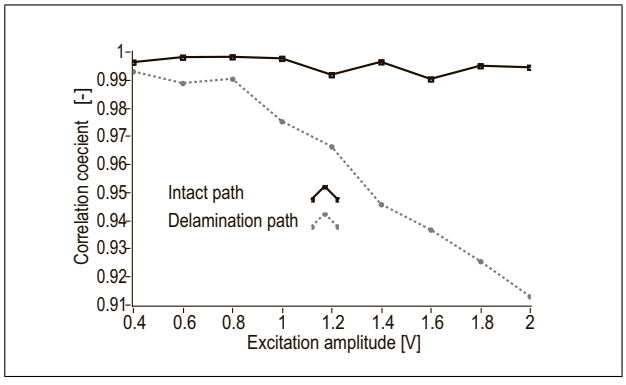

Figure 10. Correlation coefficient or coherence evaluation (Equation 14) over the intact (T1R5) and delaminated paths (T3R7) as function of the different excitation amplitude levels, indicating an increase in phase variation with increasing excitation amplitude.

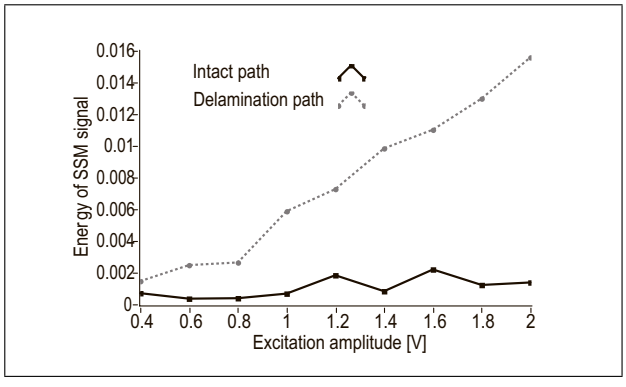

Figure 11. Energy of the SSM signal evaluation (Equation 15) over the intact (T1R5) and delaminated paths (T3R7) as function of the different excitation amplitude levels, calculated after amplitude compensation.

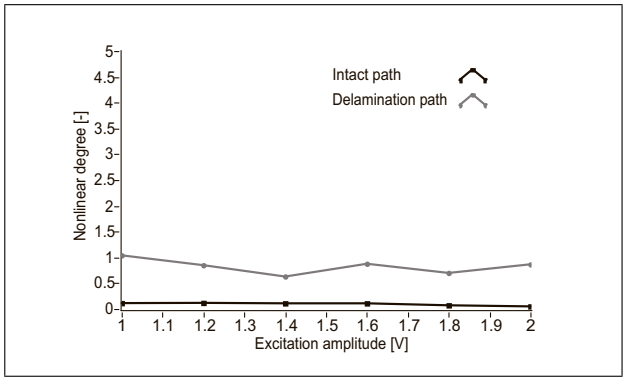

Figure 12. Third Harmonic Ratio signature (Equation 16) as function of the different excitation amplitude levels analyzed for the intact (T1R5) and delaminated paths (T3R7), showing that the presence of a delamination induces the generation of a significant third harmonic component.

7. Nonlinear variant of RAPID: NSDC based defect images

The selection of the optimal pitch-catch defect frequency and the search for optimal damage sensitive parameters discussed in the previous sections will now be incorporated into a novel nonlinear Lamb wave based imaging concept, using the full set of sparse array network measurements.

7.1. General algorithm

As in linear RAPID [6, 7], we first define a 2D spatial distribution function in order to extrapolate the individual NSDC value for a particular direct path to the area along the direct propagation path between the transmitter and receiver [33],

$$\begin{cases} \mathrm{SDF}_{ij}(x,y) = \dfrac{\beta - R_{ij}(x,y)}{\beta - 1} & \text{for } \beta > R_{ij}(x,y), \\ \mathrm{SDF}_{ij}(x,y) = 0 & \text{for } \beta \le R_{ij}(x,y), \end{cases} \tag{18}$$

where β is the shape parameter, (x, y) the coordinates of the mesh point and

$$R_{ij}(x,y) = \frac{\sqrt{(x_i - x)^2 + (y_i - y)^2} + \sqrt{(x_j - x)^2 + (y_j - y)^2}}{\sqrt{(x_j - x_i)^2 + (y_j - y_i)^2}} \tag{19}$$

the ratio of the sum of the distances from the transmitter and the receiver to point (x, y), to the distance between transmitter and receiver. Note that the value of the parameter β controls the width of the ellipse: the closer the value of β is to 1, the smaller the transverse size of the ellipse. In the present research study, the value of β is chosen equal to 1.015.

Next, to obtain a probability map for the presence of damage, we multiply the NSDC_{ij} value with the appropriate distribution $\mathrm{SDF}_{ij}(x, y)$ for all transducer-receiver pairs, and sum these partial contributions all together. Doing so, the final formula for the damage presence probability at the mesh point (x, y) reads

$$P_{xy} = \sum_{i=1}^{N} \sum_{j=1, j\neq i}^{N} \mathrm{NSDC}_{ij} \mathrm{SDF}_{ij}(x,y), \tag{20}$$

where N is the total number of transducers in the sparse array. Probabilistic images can now be constructed by accounting for the new NSDC options, defined by way of the correlation coefficient (6), the energy of the SSM signal (11) or the third harmonic ratio (12).

7.2. Validation experiment

In the current study applied to the composite plate with a $20 \times 20\,\mathrm{mm}^2$ delamination (Section 3), the input signal for the round-robin test is tuned to 378 kHz as this was found to be the optimal pitch-catch defect frequency. There are 9 transducers/sensors in the network. Only the response signals at 0.2 V and 2 V have been used in the reconstruction.

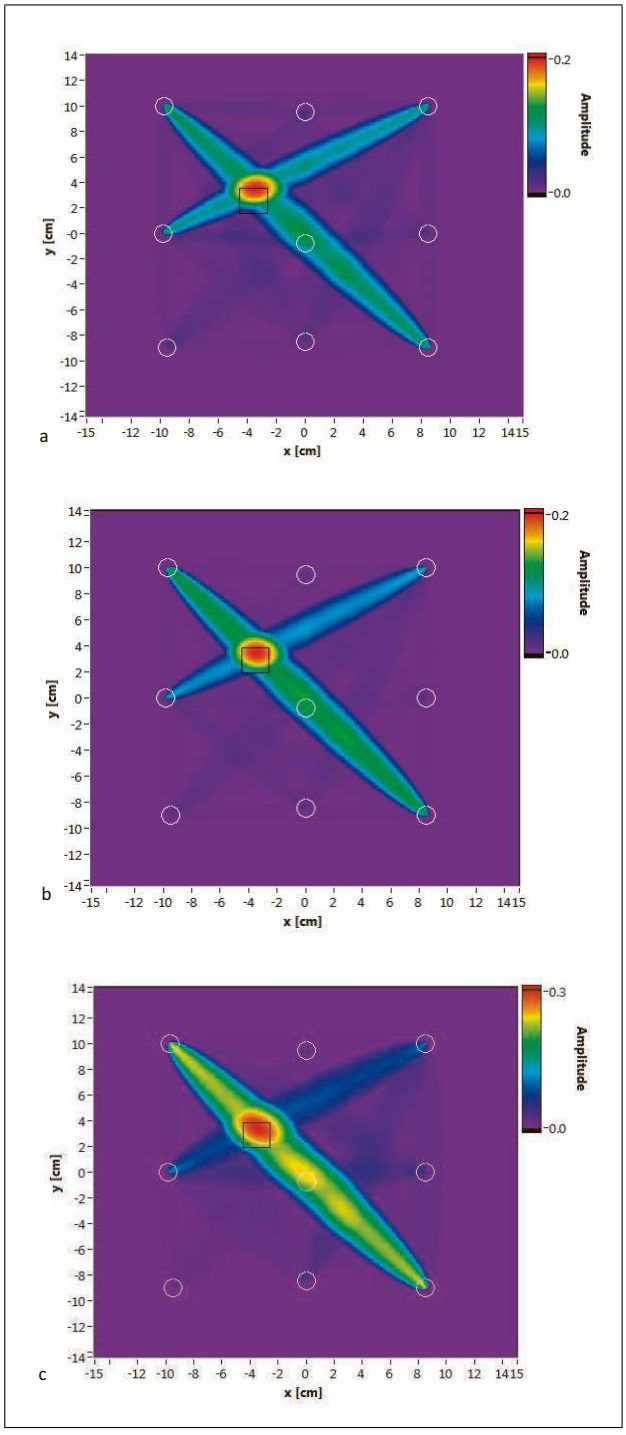

Figure 13. (Colour online) Nonlinear Lamb wave based defect imaging using the nonlinear variant of the RAPID technique, using an excitation frequency of 378 kHz, in combination with a) the high–low signal correlation coefficient, b) the energy of the SSM signals, c) the third harmonic ratio signature.

Figures 13a, b and c show the nonlinear Lamb wave based images obtained by applying RAPID with the three aforementioned nonlinear signal difference coefficients. The actual location of the defect is marked by a square on the figure, superimposed on the image. The positions of the transducers are indicated by means of white circles. In all cases, the location of the defect is clearly identified.

We generally obtain an error of maximum 1 cm for the defect location. However, it is fairly obvious that this error can be decreased by using more transducers in the sparse array network.

8. Conclusion

A new concept for defect localization based on nonlinear signal difference coefficient imaging within a sparse array of transducers has been discussed in this research. In order to reconstruct a proper defect related image, we first developed a procedure to select the most sensitive frequency to detect the defect. The pitch-catch optimal frequency selection technique showed that there is a range of frequencies which exhibit a high sensitivity to the presence of internal defects (delamination) in a composite structure. These frequencies are characterized by strong attenuation of the out-of-plane displacement in the dominant S_0 mode. Next, three nonlinearity parameters, including the high-low signal correlation coefficient, the energy of the SSM signal, and the third harmonic ratio, were identified and evaluated for the assessment of the nonclassical nonlinear (hysteretic) behavior of a delamination in different paths of the sparse array network. It was found that all three nonlinearity parameters exhibited a sufficient damage sensitivity, and that the high-low signal correlation coefficient and the energy of the SSM signals are most sensitive to phase shifts in the signal. Finally, defect imaging was demonstrated by the probabilistic imaging (RAPID) technique in combination with the three proposed nonlinearity parameters. The results demonstrate the potential of this technique in estimating damage locations with an acceptable error for each of the considered parameters.

The major advantages of the new concept are 1) that it is highly damage selective as only the presence of nonlinearity (i.e. damage) yields non zero signal difference coefficients, and 2) that it is essentially a base-line free method in the sense that no information on the intact state is necessary. The lowest excitation amplitude response plays the role of reference signal. When properly automated, all measurements can be made quickly under the same circumstances, eliminating the effects of environmental factors such as humidity or temperature. In this respect, analysis can be performed at many different frequencies in a short time which makes the selection of an optimal excitation frequency less critical. Due to the robustness of the method, data fusion of the images collected for several frequencies (or frequency ranges) should provide a clear picture of the damage distribution.

Acknowledgments

The research leading to these results has gratefully received funding from the European Union Seventh Framework Programme (FP7/2007-2013) for research, technological development and demonstration under the Grant Agreements no. 284562 (SARISTU) and no. 314768 (ALAMSA). The authors would also like to thank Prof. Alessandro Marzani from university of Bologna for granting a free license to use GUIGUW in order to create theoretical dispersion curves.

References

[1] N. Krohn, R. Stoessel, G. Busse: Acoustic non-linearity for defect selective imaging. Ultrasonics **40** (2002) 633–637.

[2] I. Solodov, J. Bai, S. Bekgulyan, et al.: A local defect resonance to enhance acoustic wave-defect interaction in ultrasonic nondestructive evaluation. Appl Phys Lett **99** (2011) 211911–211911–3.

[3] T. J. Ulrich, P. A. Johnson, A. Sutin: Imaging nonlinear scatterers applying the time reversal mirror. J Acoust Soc Am **119** (2006) 1514–1518.

[4] V. V. Kazakov, A. Sutin, P. A. Johnson: Sensitive imaging of an elastic nonlinear wave-scattering source in a solid. Appl Phys Lett **81** (2002) 646–648.

[5] Y. Ohara, S. Yamamoto, T. Mihara, et al.: Ultrasonic evaluation of closed cracks using subharmonic phased array. Jpn J Appl Phys **47** (2008) 3908–3915.

[6] H. Gao, Y. Shi, J. L. Rose: Guided wave tomography on an aircraft wing with leave in place sensors. AIP Conf Proc, 2005, 760: 1788–1794.

[7] X. Zhao, T. Qian, G. Mei, et al.: Active health monitoring of an aircraft wing with an embedded piezoelectric sensor/actuator network. II: Wireless approaches. Smart Mater Struct **16** (2007) 1218–1225.

[8] R. A. Guyer, P. A. Johnson: Nonlinear mesoscopic elasticity: Evidence for a new class of materials. Phys Today **52** (1999) 30–36.

[9] M. Scalerandi: Power laws and elastic nonlinearity in materials with complex microstructure. Phys Lett A **380** (2016) 413–421.

[10] K. R. McCall, R. A. Guyer: Equation of state and wave propagation in hysteretic nonlinear elastic materials. Journal of Geophysical Research: Solid Earth **99** (1994) 23887–23897.

[11] S. Haupert, G. Renaud, J. Rivière, et al.: High-accuracy acoustic detection of nonclassical component of material nonlinearity. J Acoust Soc Am **130** (2011) 2654–2661.

[12] P. P. Delsanto: Universality of nonclassical nonlinearity: Applications to non-destructive evaluations and ultrasonics. Springer, 2007.

[13] H. Gerhard, G. Busse: Deformation-measurement with speckle-interferometry by ultrasound excitation. NDT.net.

[14] K. E. Van Den Abeele, A. Sutin, J. Carmeliet, et al.: Micro-damage diagnostics using nonlinear elastic wave spectroscopy (NEWS). NDT E Int **34** (2001) 239–248.

[15] C. Payan, T. J. Ulrich, P. Y. Le Bas, et al.: Quantitative linear and nonlinear resonance inspection techniques and analysis for material characterization: Application to concrete thermal damage. J Acoust Soc Am **136** (2014) 537–547.

[16] K. E.-A. Van Den Abeele, P. A. Johnson, R. A. Guyer, et al.: On the quasi-analytic treatment of hysteretic nonlinear response in elastic wave propagation. J Acoust Soc Am **101** (1997) 1885–1898.

[17] V. V. Kazakov, P. A. Johnson: Nonlinear wave modulation imaging. 2. 763-766.

[18] I. Solodov, D. Döring: New opportunities for NDT using non-linear interaction of elastic waves with defects. In: Nonlinear Acoustics at the Beginning of the 21st Century. O. V. Rudenko, O. A. Sapozhnikov (eds.). J Mech Eng **57** (2011) 169–182.

[19] C. Pecorari, I. Solodov: Nonclassical nonlinear dynamics of solid interfaces in partial contact for NDE applications.

Universality of non-classical nonlinearity with application to NDE and ultrasonics. Springer Verlag, New York, 2006. 307-324.

[20] I. Solodov: Nonlinear acoustic NDT: Approaches, methods, and applications. 5th International Workshop NDT in Progress, October 12–14, 2009.

[21] S. Vanaverbeke, K. Van Den Abeele: Two-dimensional modeling of wave propagation in materials with hysteretic nonlinearity. J Acoust Soc Am **122** (2007) 58–72.

[22] E. Barbieri, M. Meo, U. Polimeno: Nonlinear wave propagation in damaged hysteretic materials using a frequency domain-based PM space formulation. Int J Solids Struct **46** (2009) 165–180.

[23] K. Van Den Abeele, P. A. Johnson, A. Sutin: Nonlinear elastic wave spectroscopy (NEWS) techniques to discern material damage. Part I: Nonlinear wave modulation spectroscopy (NWMS). Res Nondestruct Eval **12** (2000) 17–30.

[24] http://www.guiguw.com/.

[25] D. Alleyne, P. Cawley: A two-dimensional fourier transform method for measurement of propagating multimode signals. J Acoust Soc Am **89** (1991) 1159–1168.

[26] V. Giurgiutiu: Tuned Lamb wave excitation and detection with piezoelectric wafer active sensors for structural health monitoring. J Intell Mater Syst Struct **16** (2005) 291–305.

[27] V. Giurgiutiu, G. Santoni-Bottai: Structural health monitoring of composite structures with piezoelectric-wafer active sensors. AIAA J **49** (2011) 565–581.

[28] J. Pohl, C. Willberg, U. Gabbert, et al.: Experimental and theoretical analysis of Lamb wave generation by piezoceramic actuators for structural health monitoring. Exp Mech **52** (2012) 429–438.

[29] P. D. Wilcox, R. P. Dalton, M. J. S. Lowe, et al.: Mode and transducer selection for long range Lamb wave inspection. Key Eng Mater **167-168** (1999) 152–161.

[30] O. Mesnil, C. A. Leckey, M. Ruzzene: Instantaneous and local wavenumber estimations for damage quantification in composites. Struct Heal Monit (2014) 1–12.

[31] C. L. E. Bruno, A. S. Gliozzi, M. Scalerandi, et al.: Analysis of elastic nonlinearity using the scaling subtraction method. Phys Rev B - Condens Matter Mater Phys **79** (2009) 064108(1–13).

[32] J. Rivière, S. Haupert, P. Laugier, et al.: Nonlinear ultrasound: Potential of the cross-correlation method for osseointegration monitoring. J Acoust Soc Am **132** (2012) EL202.

[33] T. R. Hay, R. L. Royer, H. Gao, et al.: A comparison of embedded sensor Lamb wave ultrasonic tomography approaches for material loss detection. Smart Mater Struct **15** (2006) 946–951.